IEEE Access
Multidisciplinary | Rapid Review | Open Access Journal

Received 13 July 2023, accepted 7 August 2023, date of publication 10 August 2023, date of current version 17 August 2023.

Digital Object Identifier 10.1109/ACCESS.2023.3304017

RESEARCH ARTICLE

Brushless Wound Rotor Vernier Motor Using Single-Phase Additional Winding on Stator for Variable Speed Applications

MUHAMMAD HUMZA[1], TANVEER YAZDAN[2], MUDASSIR RAZA SIDDIQI[3], AND HAN-WOOK CHO[1], (Member, IEEE)

[1]Department of Electrical, Electronics, and Communication Engineering Education, Chungnam National University, Daejeon 34134, Republic of Korea
[2]Department of Electrical Engineering, The University of Lahore, Lahore 54000, Pakistan
[3]Department of Electrical Engineering, Incheon National University, Incheon 22012, Republic of Korea

Corresponding authors: Han-Wook Cho (hwcho@cnu.ac.kr) and Tanveer Yazdan (tanveeryazdan23@gmail.com)

This work was supported by the research fund of Chungnam National University, Daejeon, Republic of Korea.

ABSTRACT This paper introduces a topology for achieving the brushless operation of a wound rotor vernier motor using a single-phase additional winding on the stator, specifically designed for variable-speed applications e.g., washing machines. In the proposed topology, the stator winding consists of two sets: a four-pole three-phase main winding and an additional two-pole single-phase winding. On the other hand, the rotor contains a 44-pole field winding to generate the vernier effect, and a two-pole excitation winding for induction. The main winding of the stator produces the fundamental component of MMF, while the additional winding generates the subharmonics component of MMF to induce a current in the excitation winding of the rotor. The excitation winding is connected to a rotating rectifier to supply direct current to the rotor's field winding. The field interaction of the main and field winding is responsible for the production of torque. The presence of a subharmonic component of MMF in the air gap is confirmed through Fourier analysis of MMF obtained from the winding function. Moreover, the brushless operation of the proposed topology is validated using 2D finite element analysis (FEM) for variable speed application.

INDEX TERMS Brushless operation, single-phase additional winding, subharmonic generation, wound rotor vernier motor.

I. INTRODUCTION

Permanent magnet vernier machines (PMVMs) have garnered significant attention in recent decades due to their ability to provide high torque density for direct drive systems. These machines offer the benefit of low noise and maintenance by eliminating the mechanical gear system desired in various applications [1]. Whereas their usage in variable-speed applications is limited due to increased core losses and reactance at high speeds, which imposes limitations on the inverters [2], [3]. Since PMVMs are known for their ability to generate an additional active flux wave through the stator slot harmonic component of airgap permeance, in addition to the common flux wave seen in conventional PM motors. This enables them to produce two to three times higher back-EMF and torque, depending on the magnitude of the slot harmonic components of permeance. To maximize these slot harmonic components, it is crucial to minimize the effective airgap length. However, in SPM vernier motors, the magnet thickness increases the effective gap length, thereby reducing the slot harmonic permeance. Hence, a trade-off arises between MMF (magneto-motive force) and slot harmonics when selecting the magnet thickness, which affects the back electromotive force (EMF) of the motor. Whereas the use of thin magnets enhances the chances of demagnetization. To overcome these issues, the spoke-type magnet structure is employed, however, this topology exhibits magnetic potential oscillations in the rotor core which suppress the vernier effect [4]. Moreover, the high cost of PMVMs is attributed to the use of rare-earth permanent magnets [5], [6], compelling

The associate editor coordinating the review of this manuscript and approving it for publication was Giambattista Gruosso.

the researchers to explore magnet-free and cost-effective alternatives in machine design.

Among these machines, the reluctance vernier machines (VRMs) offer a more affordable solution compared to PMVMs since they do not require permanent magnets for exciting the rotor field. These VRMs suffer from the drawback of low torque density [7]. To improve the torque density of VRMs, direct current vernier reluctance machines (DC-VRMs) have been introduced, incorporating field windings on the stator to improve durability and reduce cost [8], [9], [10]. However, this approach resulted in significant stator saturation and limitations on the fill factor and the current density of the armature winding. In response to these issues, wound-rotor vernier machines have been proposed, placing the field windings on the rotor instead of the stator [11], [12]. Such designs reduce the saturation levels and the air gap length by eliminating the magnets which benefit enhanced slot harmonics permeance to achieve a higher modulation effect. These wound rotor vernier machines pose the challenges of maintaining the brushes and slip rings necessary for rotor excitation.

To resolve these challenges, researchers are currently exploring various brushless configurations for wound rotor vernier machines [13], [14], [15], [16], [17]. These configurations generate an additional harmonic component of MMF of the stator along with the fundamental component and utilize this harmonic component for field excitation to achieve brushless operation demanding dual inverters at the input. The use of dual three-phase inverters increases the control complexity and the cost. Therefore, it is a need for a reduction in cost and control complexity associated with the inverters in these techniques, particularly for variable speed applications.

In this paper, a brushless wound rotor vernier topology using an additional single-phase stator winding is presented for variable speed applications. The stator of the machine is comprised of two sets of winding (a) four-pole three-phase main winding (ABC winding) supplied with current from a three-phase inverter, and (b) an additional two-pole single-phase winding (A2 winding) supplied with current from the single-phase inverter. On the other hand, the rotor of the machine also has two sets of winding (i) two-pole excitation winding and (ii) forty-four-pole field winding. For operation, the main winding of the stator will generate the fundamental component of MMF while additional winding is responsible for the generation of the sub-harmonic component of MMF in the airgap. In order to determine these harmonic components, Fourier analysis of the MMF waveform generated by the stator winding has been performed. This analysis demonstrated that the proposed machine exhibits a higher magnitude of the subharmonic component. As a result, it facilitates improved induction in the excitation winding of the rotor, leading to increased current flow in it. This excitation winding supplies direct current (DC) to the field winding of the rotor through a bridge rectifier mounted on the shaft. This field current will interact with the field of the main winding of the stator to generate the torque. To validate the performance of the motor, a 2D FEM analysis is performed for the application of the washing machine.

II. MACHINE TOPOLOGIES AND OPERATING PRINCIPLE

The slot and pole combination of the vernier motor is given by (1)

$$Z_r = Z_s \pm p \tag{1}$$

where Z_r is the rotor pole pairs, Z_s is the stator slots and p is the stator winding pole pairs. In this paper, 24 slots and 2 winding pole pairs on the stator are chosen, which yields the 22 rotor pole pairs satisfying (1).

A. REFERENCE MACHINE TOPOLOGY

The topology for the reference motor is shown in Fig. 1 having dual winding on the stator and the rotor for the brushless operation.

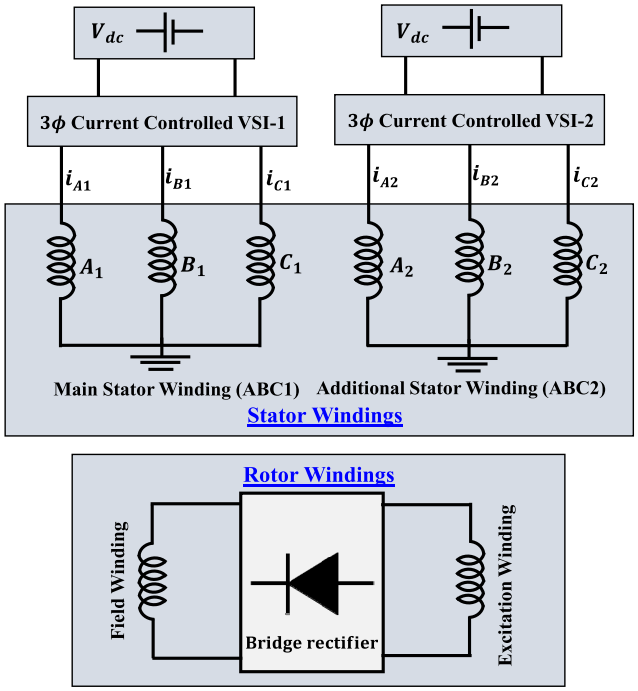

FIGURE 1. Reference brushless machine topology.

In this configuration, the stator winding is incorporated with two separate windings: (a) the main winding (ABC1) making four poles, and (b) an additional winding (ABC2) forming two poles. The configuration of both windings is depicted in Fig. 2, where ABC1 occupies 18 slots and ABC2 occupies 6 slots.

The winding ABC1 is energized by a three-phase inverter (VSI-1) to generate the fundamental component of the MMF and ABC2 is powered by another three-phase inverter (VSI-2), responsible for generating the sub-harmonic component of the MMF. The output currents from these three-phase

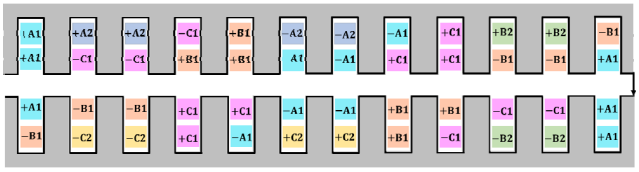

FIGURE 2. Stator winding layout used for the reference machine.

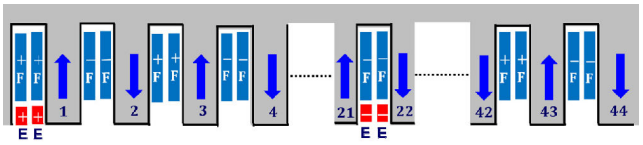

FIGURE 3. Rotor winding layout.

inverters for reference motor are given by (2) & (3)

$$i_{ABC1} = I_{mag} \sin\left(\omega t - m\frac{2\pi}{3}\right) \tag{2}$$

$$i_{ABC2} = I_{mag} \sin\left(\omega t - n\frac{2\pi}{3}\right) \tag{3}$$

where, i_{ABC1} and i_{ABC2} are the three-phase currents supplied to the ABC1 and ABC2 winding respectively, $m = 0, 1, 2$ for phases A1, B1, and C1 respectively, $n = 0, 1, 2$ for phases A2, B2, and C2, with I_{mag} is the magnitude of current, ω is the angular frequency, and t is the time.

The winding functions for both winding sets are given by (4) & (5)

$$N_{ABC1}(\varphi) = \frac{4N_1}{\pi} \cos\left(\varphi - m\frac{2\pi}{3}\right) \tag{4}$$

$$N_{ABC2}(\varphi) = \frac{2N_2}{\pi} \cos\left(\left(\frac{\varphi - n\frac{2\pi}{3}}{2}\right)\right) \tag{5}$$

where, N_1 and N_2 are turns per phase of ABC1 and ABC2 windings, respectively.

The MMF for the reference machine based on the winding function and currents is given by (6)

$$F_{Ref}(\varphi, i) = \left\{ \begin{array}{l} \frac{4N_1 I_{mag}}{\pi} \left(\sum_{m=0}^{2} \cos\left(\varphi - m\frac{2\pi}{3}\right) \sin\left(\omega t - m\frac{2\pi}{3}\right) \right) + \\ \frac{2N_2 I_{mag}}{\pi} \left(\sum_{n=0}^{2} \cos\left(\frac{\varphi - n\frac{2\pi}{3}}{2}\right) \sin\left(\omega t - n\frac{2\pi}{3}\right) \right) \end{array} \right\} \tag{6}$$

The above equation consists of two terms: the first term corresponds to the fundamental component of MMF responsible for generating the torque, while the second term represents the subharmonic components of MMF. This subharmonic component is utilized to induce the current in the rotor excitation winding, enabling the brushless operation of the machine.

Similarly, the rotor of the machine consists of two distinct winding types illustrated in Fig. 3, (i) excitation winding forming two poles and (ii) field winding forming 44 poles.

The excitation winding is inductively coupled with the ABC2 winding of the stator to receive the subharmonic current. Further, the rotating rectifier converts the induced AC of excitation winding to DC required for field winding.

The resulting MMF waveform is shown in Fig. 4 (a), and its Fourier analysis is performed to determine the magnitudes of the fundamental and subharmonic components, as depicted in Fig. 4 (b). The analysis reveals that the magnitude of the subharmonic component is 33.5 % of the fundamental component.

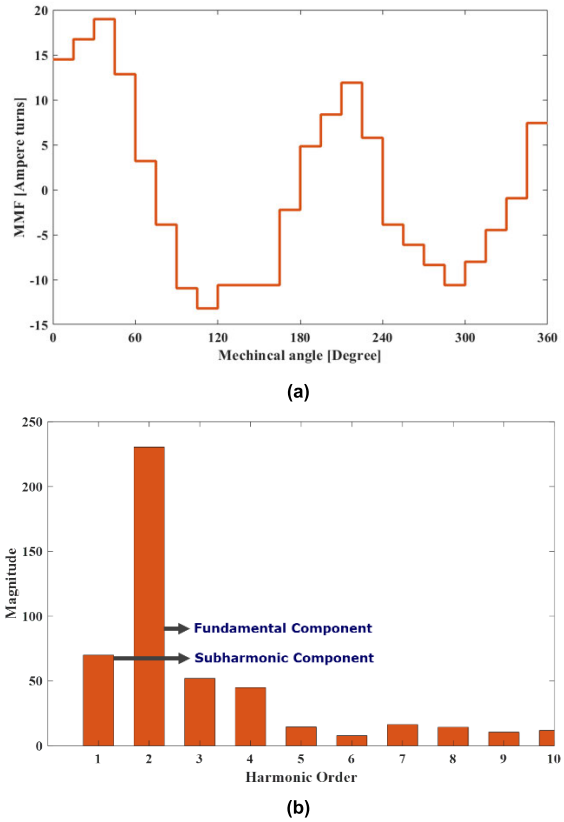

FIGURE 4. Reference brushless machine (a) stator winding MMF (b) harmonic contents in MMF.

The rotational speeds of these components of the MMF can be calculated using (7)

$$N_S(h) = \frac{120 \times f}{h \times p} \tag{7}$$

where $N_S(h)$ represents the rotational speed of the harmonic component, h denotes the harmonic number, f is the input supply frequency and P represents the number of poles. Equation (7) reveals that the fundamental and subharmonic components rotate at different speeds. Consequently, it can be inferred that the subharmonic component is asynchronous with the fundamental component, facilitating its induction in the rotor excitation winding for brushless excitation.

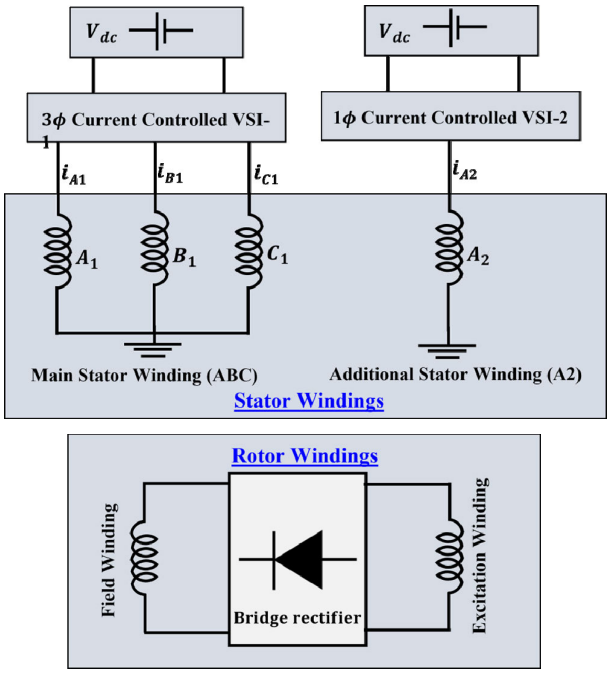

FIGURE 5. Proposed brushless topology.

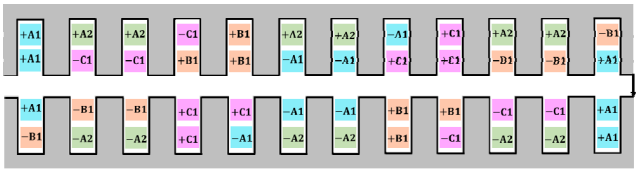

FIGURE 6. Stator winding layout used for the proposed machine.

B. PROPOSED MACHINE TOPOLOGY

The topology of brushless operation in the proposed machine is shown in Fig. 5.

It consists of two separate windings, similar to the reference motor, however, with some distinctions. The main winding (ABC) is of the three-phase forming four poles, while the additional winding (A2) is a single-phase forming two poles.

The arrangement of winding for the proposed machine is presented in Fig. 6, showcasing the allocation of 18 slots for the winding ABC, while the remaining 6 slots are used for winding A2.

In this configuration, the winding ABC is supplied using the three-phase inverter (VSI-1) to generate the fundamental component of MMF, while the winding A2 is energized through the single-phase inverter (SVI-2) to produce the subharmonic component of the net MMF.

The output currents from these inverters for the proposed motor are given by (8) & (9)

$$i_{ABC} = I_{mag} \sin\left(\omega t - m\frac{2\pi}{3}\right) \tag{8}$$

$$i_{A2} = I_{mag} \sin\left(\omega t\right) \tag{9}$$

where i_{A2} is the current supplied to the single-phase winding of the stator.

The winding functions $N_{ABC}(\varphi)$ and $N_{A2}(\varphi)$ for both stator windings of the proposed motor are given by (10) & (11)

$$N_{ABC}\left(\varphi\right) = \frac{4N_1}{\pi} \cos\left(\varphi - m\frac{2\pi}{3}\right) \tag{10}$$

$$N_{A2}\left(\varphi\right) = \frac{2N_2}{\pi} \cos\left(\frac{\varphi}{2}\right) \tag{11}$$

The resulting MMF for the proposed machine will be.

$$F_{Pro}\left(\varphi, i\right) = \left\{ \begin{array}{l} \frac{4N_1 I_{mag}}{\pi}\left(\sum_{m=0}^{2} \cos\left(\varphi - m\frac{2\pi}{3}\right) \sin\left(\omega t - m\frac{2\pi}{3}\right)\right) + \\ \frac{2N_2 I_{mag}}{\pi}\left(\cos\left(\frac{\varphi}{2}\right) \sin\left(\omega t\right)\right) \end{array} \right\} \tag{12}$$

In this equation, the first term represents the fundamental component of the MMF used to generate torque. Conversely, the second term corresponds to the subharmonic component of the MMF. This component induces a current in the rotor enabling the brushless excitation keeping the same rotor configuration as in the reference motor.

To validate the generation of the subharmonic component in the proposed topology using the additional single-phase (A2) winding, the MMF of the stator is analyzed via Fourier analysis and compared to that of the reference machine under the conditions of the same input current. Fig. 7 (a) shows the resulting waveform of the MMF, while Fig. 7 (b) displays the harmonic contents, indicating that the subharmonic component accounts for 79% of the fundamental component. It is noteworthy that the subharmonic component in the proposed machine is more than twice that of the reference machine. Therefore, the proposed machine will offer enhanced induction capabilities through the utilization of this subharmonic component. However, the magnitude of the fundamental component is reduced by approximately 15% compared to the reference machine. These findings imply that achieving the same level of field current and output torque of the reference machine will require a 15% higher current for the main winding and more than two times less current for the additional winding.

The overall illustration of the operating principle of these machines in a comprehensive way is given in Fig. 8.

III. 2D-FEM SIMULATIONS AND RESULTS

To validate the proposed topology for the application of washing machine, reference and proposed models of wound rotor brushless vernier motors with outer rotors are developed and analyzed in 2D-FEM. The design parameters of both machines were kept the same for a fair comparison of their performance characteristics and are given in Table 1.

These motors can be operated in variable-speed applications by controlling the current of the main and additional winding, keeping the output power of the machine constant.

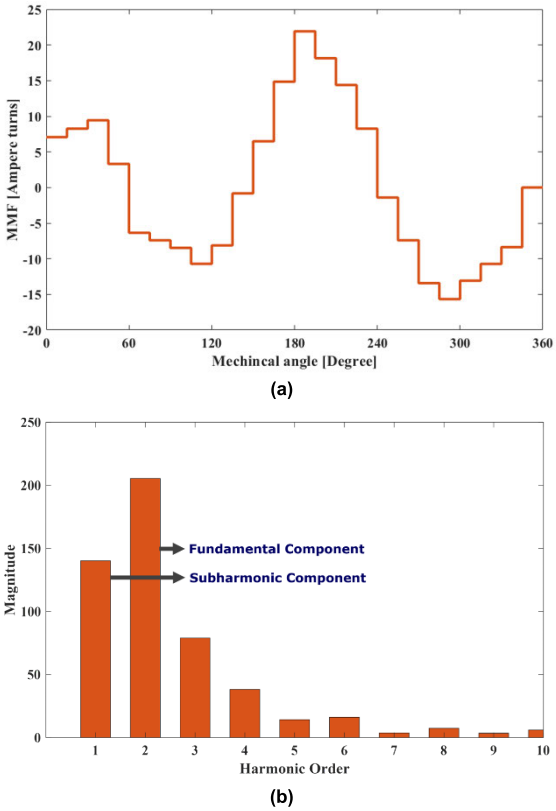

FIGURE 7. Proposed brushless machine (a) stator winding MMF (b) harmonic contents in MMF.

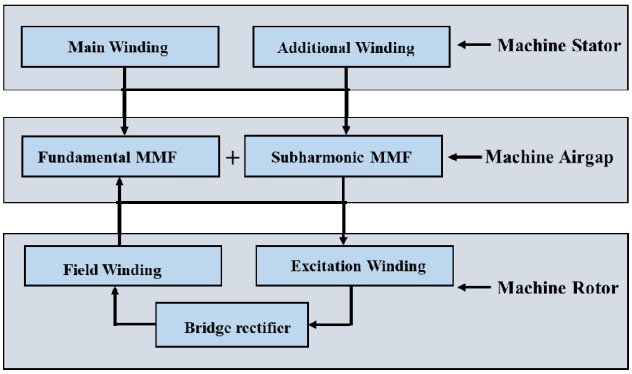

FIGURE 8. Comprehensive illustration of operating principle.

However, in this paper, only the main winding current is controlled for achieving the washing and spin mode of the washing machine application.

A. NO-LOAD ANALYSIS

Under the same design constraints, no-load analysis is performed by applying a direct current of 6.5A to the field winding at a speed of 530 rpm in washing mode. The no-load characteristics for both machines are identical and the generated back-EMF for any of these motors is shown in Fig. 9, with the RMS value of 59.5V.

TABLE 1. Design parameters of machines.

Parameters	Units	Value
Rated power	W	500
Washing mode Speed	rpm	530
Spinning mode Speed	rpm	1200
Stator I/O diameter	mm	50/95.5
Rotor I/O diameter	mm	96/150
Stack length	mm	100
Airgap length	mm	0.5
Number of stator slots	-	24
Number of rotor slots	-	44
Stator winding poles	-	02/04
Excitation/Field winding poles	-	02/44
Stator's No. of turns/slot	-	18
Field winding's No. of turns/slot	-	15
Excitation winding total turns	-	10

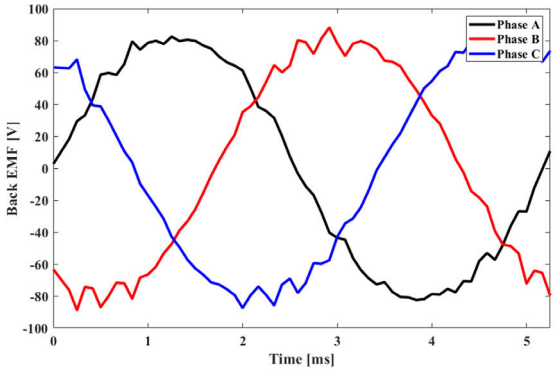

FIGURE 9. No-load back EMF.

Further, the flux density distribution in the machine is illustrated in Fig. 10. It can be observed that the teeth of the machine exhibit a maximum flux density of 0.867 T, which is in a reasonable range without saturation.

Further, the performance characteristics are investigated in washing and spin mode for these motors.

B. ANALYSIS IN WASHING MODE

In the washing mode at speed of 530 rpm, the reference machine has been supplied with a 3.45 A_{pk} current to both the ABC1 and ABC2 windings using their respective inverters. In order to maintain the same field current and torque production, the input currents of the proposed machine were calculated based on their respective MMF component values relative to those of the reference machine. Therefore, the input currents applied to the windings ABC and A2 of the proposed machine are 4.1 A_{pk} and 1.52 A_{pk}, respectively.

The presence of the additional winding (ABC2 or A2) induces a voltage in the excitation winding of the rotor, serving as an input source for the rotating rectifier, which converts the AC input into a DC supply for the field winding. The resulting rotor currents for both machines under steady-state conditions are shown in Fig. 11 (a) and Fig. 11 (b). The RMS values of the excitation currents are 4.8 A and 4.07 A, while the field currents are 6.5 A_{dc} and 6.48 A_{dc} in the

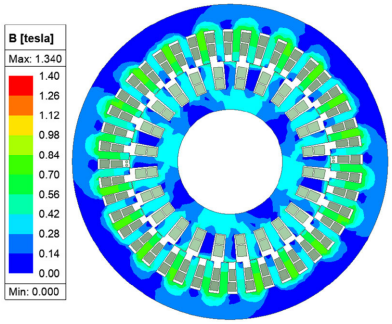

FIGURE 10. Flux density distribution at no-load condition.

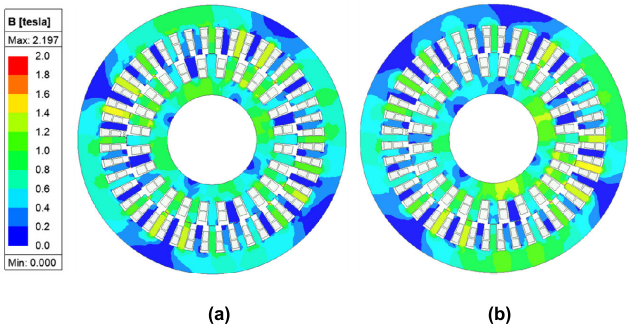

FIGURE 12. Flux density distribution for washing mode (a) reference machine (b) proposed machine.

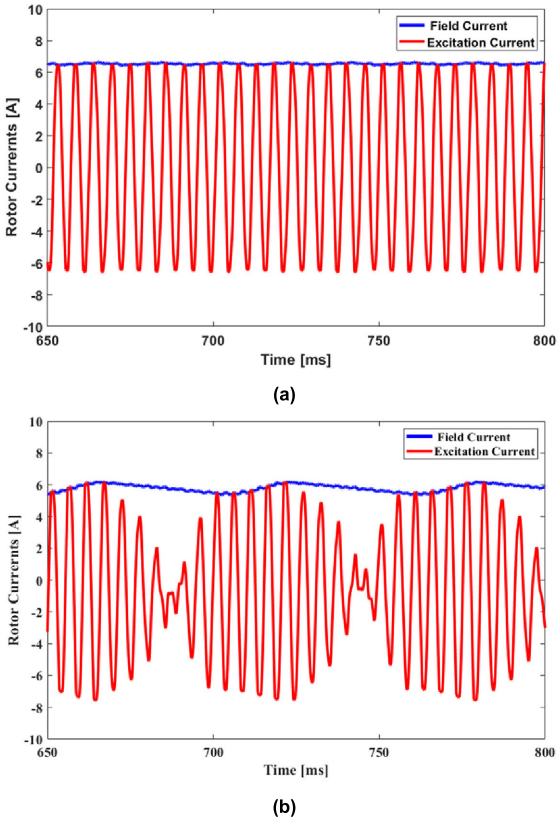

FIGURE 11. Rotor currents for washing mode (a) reference machine (b) proposed machine.

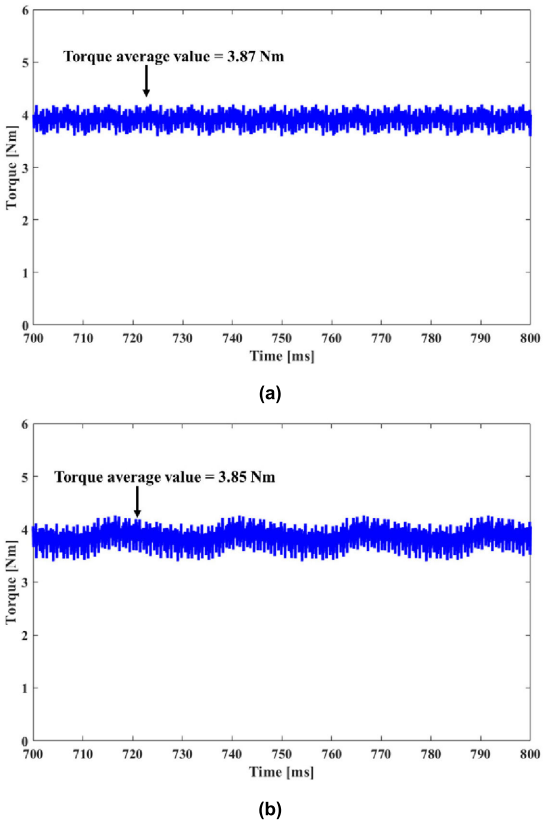

FIGURE 13. Output torque for washing mode (a) reference machine (b) proposed machine.

reference and proposed machines, respectively. The results confirm the achieving of similar field currents through the induction phenomenon in these machines.

Owing to the flow of these currents, the flux density distribution is illustrated in Fig. 12, which shows the maximum values of 1.65 T and 1.46 T for the reference and proposed machines, respectively. Although the flux density in the reference machine is higher due to its higher input current. However, it is important to emphasize that both values are within a reasonable and acceptable range under the saturation.

The field of the rotor interacts with the main field of the stator to generate torque. The torque outputs of both machines are presented in Fig. 13 (a) and Fig. 13 (b), and its average values for the reference and proposed machines are 9.16 Nm and 9.15 Nm, with torque ripples of 9.34 % and 17.68 %, respectively. It is observed that both machines exhibit the same torque, while the torque ripples of the proposed machine are quite larger due to single-phase excitation for subharmonic generation.

Moreover, the efficiencies of both machines have been evaluated by considering the core and the copper losses. The copper losses are determined to be 36.72 W and 37.32 W, while the core losses as 90.5 W and 84.8 W for the reference and proposed machines, respectively. The reference machine

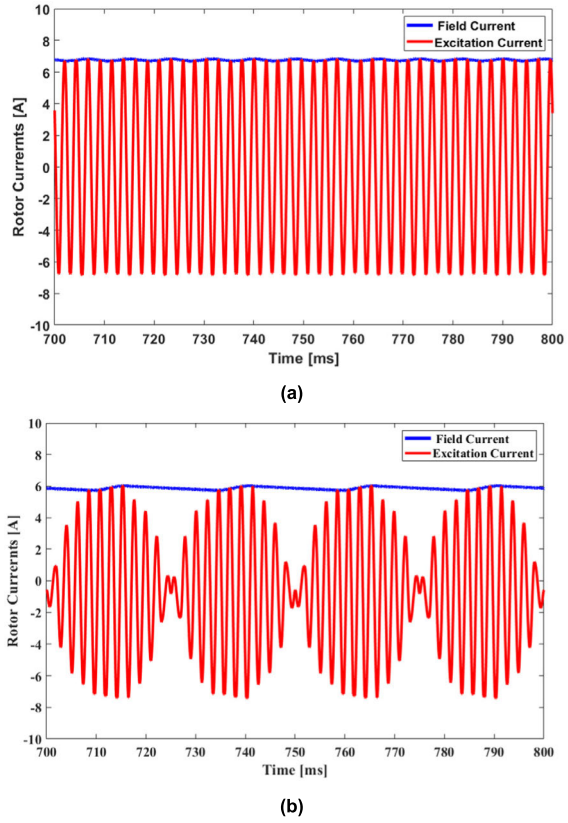

FIGURE 14. Rotor currents for spin mode (a) reference machine (b) proposed machine.

exhibits more core losses due to overall higher input current to the stator. Based on these losses, the efficiencies of these machines are calculated as 74.98 % and 75.95 %. The efficiency of the proposed machine in washing mode is slightly better due to decreased core losses.

C. ANALYSIS IN SPIN MODE

For the spin mode, both machines are simulated at 1200 rpm. To analyze the characteristics, the phase angle of the main winding current was controlled considering the inverter voltage rating. During this operation at high speed, the reactance of the vernier motor increases rapidly which reduces the current in the main winding. Due to this reason, the peak currents drawn by the main winding of the reference and the proposed machines are 3.3 A and 3.75 A at maximum input voltage, while the currents for additional windings are 3.35 A and 1.45 A, respectively.

Through the induction phenomenon, the rotor currents for both machines operating in the spin mode are depicted in Fig. 14 (a) and Fig. 14 (b). The results of excitation currents exhibit RMS values of 4.95 A and 3.82 A, while the field currents have values of 6.77 A_{dc} and 6.57 A_{dc} for the reference and the proposed machines, respectively.

In this mode, the flux density distribution is depicted in Fig. 15, revealing the maximum flux density values of 1.125 T and 1.13 T for the reference and proposed

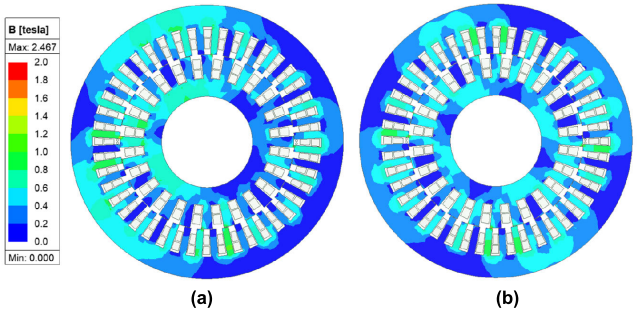

FIGURE 15. Flux density distribution for spin mode (a) reference machine (b) proposed machine.

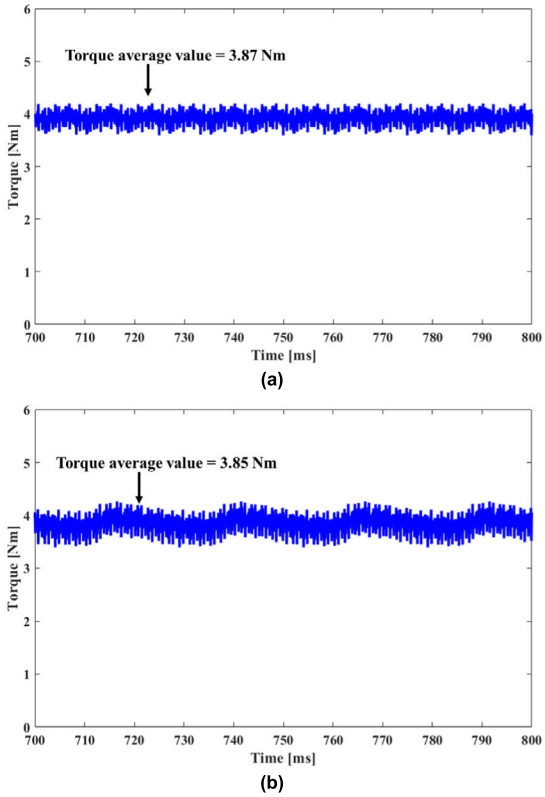

FIGURE 16. Output torque for spin mode (a) reference machine (b) proposed machine.

machines, respectively. These values remain within the acceptable range avoiding the saturation.

The output torque characteristics of both machines are shown in Fig. 16 (a) and Fig. 16 (b). The average values of torque for the reference and proposed machines are 3.87 Nm and 3.85 Nm, with torque ripples of 15.75 % and 22.48 %, respectively. The comparison shows that both machines exhibit the same torque. However, it is slightly less than 4 Nm desired for maintaining the constant power. This happens due to decreased current in the main winding because of high reactance at high speed as stated above. Moreover, the torque ripples of the proposed machine are

TABLE 2. Performance comparison.

Parameters	Units	Washing mode		Spin mode	
		Ref	Proposed	Ref	Proposed
Input I_{ABC1} current	A_{pk}	3.45	4.1	3.3	3.75
Input I_{ABC2} current	rpm	3.45	1.52	3.35	1.45
Filed current	A_{dc}	6.45	6.4	6.77	6.57
Excitation current	A_{rms}	4.8	4.1	4.95	3.82
Torque	Nm	9.16	9.15	3.87	3.85
Torque ripples	%	9.34	17.68	15.75	22.48
Copper losses	W	36.72	37.32	38.66	39.08
Core losses	W	90.5	84.8	127.5	124.23
Efficiency	%	74.98	75.95	65.83	66.24

relatively larger due to single-phase excitation for subharmonic generation.

To evaluate the efficiencies, the copper losses are calculated to be 38.66 W and 39.08 W, while the core losses are determined as 127.5 W and 124.23 W for the reference and the proposed machines, respectively. These higher core losses in reference machine are because of overall higher input current to the stator. This leads to the efficiencies of these machines being 65.83 % and 66.24 %, respectively, which shows that the proposed machine exhibits 1% more efficiency than that of the reference machine due to decreased core losses.

A comprehensive summary of the performance comparison is presented in Table 2. The comparison demonstrates that the proposed machine successfully generates an adequate amount of subharmonic, enabling improved induction for effective brushless operation with better efficiencies. This is achieved by utilizing a dedicated single-phase additional winding on the stator.

IV. CONCLUSION

This paper presented the achievement of brushless operation in a wound-rotor vernier machine by employing an additional single-phase winding on the stator to generate a subharmonic component of the stator MMF. The confirmation of this subharmonic generation through Fourier analysis provides basic information about the improved induction capabilities of the machine attributed to its enriched subharmonic component. The performance analysis revealed that the proposed machine outperforms the reference machine exhibiting 1% higher efficiency in both the washing and the spin modes. Moreover, the proposed topology offers additional benefits in terms of simplicity and cost-effectiveness by utilizing a single-phase inverter for the additional winding in brushless operation for variable-speed applications. This approach eliminates the need for the complexity of a three-phase inverter and its associated control.

As a result, the utilization of a single-phase additional winding on the stator enables brushless operation in a wound rotor vernier machine. This machine can then be applied in variable speed applications, offering improved performance.

REFERENCES

[1] B. Kim and T. A. Lipo, "Operation and design principles of a PM Vernier motor," *IEEE Trans. Ind. Appl.*, vol. 50, no. 6, pp. 3656–3663, Nov. 2014.

[2] B. Kim and T. A. Lipo, "Design of a surface PM Vernier motor for a practical variable speed application," in *Proc. IEEE Energy Convers. Congr. Expo. (ECCE)*, Montreal, QC, Canada, Sep. 2015, pp. 776–783.

[3] B. Kim, "Characteristic analysis of a Vernier PM motor considering adjustable speed control," in *Proc. IEEE Transp. Electrific. Conf. Expo, Asia–Pacific (ITEC Asia–Pacific)*, Busan, South Korea, Jun. 2016, pp. 671–676.

[4] B. Kim and T. A. Lipo, "Analysis of a PM Vernier motor with spoke structure," *IEEE Trans. Ind. Appl.*, vol. 52, no. 1, pp. 217–225, Jan. 2016.

[5] Z. S. Du and T. A. Lipo, "Efficient utilization of rare Earth permanent-magnet materials and torque ripple reduction in interior permanent-magnet machines," *IEEE Trans. Ind. Appl.*, vol. 53, no. 4, pp. 3485–3495, Jul. 2017.

[6] M. Barcaro and N. Bianchi, "Interior PM machines using ferrite to replace rare-Earth surface PM machines," *IEEE Trans. Ind. Appl.*, vol. 50, no. 2, pp. 979–985, Mar. 2014.

[7] K. C. Mukherji and A. Tustin, "Vernier reluctance motor," *Proc. Inst. Electr. Eng.*, vol. 121, no. 9, pp. 965–974, 1974.

[8] S. Jia, R. Qu, J. Li, D. Li, and H. Lu, "Comparison of stator DC current excited Vernier reluctance machines with different field winding configurations," *IEEE Trans. Magn.*, vol. 53, no. 6, pp. 1–4, Jun. 2017.

[9] S. Jia, R. Qu, J. Li, and D. Li, "Principles of stator DC winding excited Vernier reluctance machines," *IEEE Trans. Energy Convers.*, vol. 31, no. 3, pp. 935–946, Sep. 2016.

[10] X. Liu and Z. Q. Zhu, "Influence of rotor pole number on electromagnetic performance of novel variable flux reluctance machine with DC-field coil in stator," in *Proc. 7th Int. Power Electron. Motion Control Conf.*, vol. 2, Harbin, China, Jun. 2012, pp. 1108–1115.

[11] A. M. Tounzi, B. Ramdane, and M. E. Zaïm, "Study and experimentation of a rotor current excited Vernier reluctance machine aimed to direct-driven applications," *Eur. Phys. J. Appl. Phys.*, vol. 52, no. 1, p. 11102, Oct. 2010.

[12] K. Rashid, M. Azeem, and B. Kim, "Output power improvement of a Vernier motor using field winding configuration," *Int. J. Appl. Electromagn. Mech.*, vol. 64, nos. 1–4, pp. 711–719, Dec. 2020.

[13] Q. Ali, A. Hussain, N. Baloch, and B. Kwon, "Design and optimization of a brushless wound-rotor Vernier machine," *Energies*, vol. 11, no. 2, p. 317, Feb. 2018.

[14] A. Hussain, Z. Baig, W. Toor, U. Ali, M. Idrees, T. Shloul, Y. Ghadi, and H. Alkahtani, "Wound rotor synchronous motor as promising solution for traction applications," *Electronics*, vol. 11, no. 24, p. 4116, Dec. 2022.

[15] S. S. H. Bukhari, J. Ikram, F. Wang, X. Yu, J. Imtiaz, J. Rodas, and J.-S. Ro, "Novel self-excited brush-less wound field Vernier machine topology," *IEEE Access*, vol. 10, pp. 97868–97878, 2022.

[16] S. Tariq, J. Ikram, S. S. H. Bukhari, Q. Ali, A. Hussain, and J.-S. Ro, "Design and analysis of single inverter-fed brushless wound rotor Vernier machine," *IEEE Access*, vol. 10, pp. 101609–101621, 2022.

[17] S. Y. Hammad, J. Ikram, R. Badar, S. S. H. Bukhari, L. Khan, and J.-S. Ro, "Performance analysis of brushless wound rotor Vernier machine by utilizing third harmonic field excitation," *IEEE Access*, vol. 11, pp. 65480–65490, 2023.

MUHAMMAD HUMZA was born in Jampur, Punjab, Pakistan. He received the bachelor's degree in electrical engineering from the Federal Urdu University of Arts, Sciences and Technology (FUUAST), Islamabad, Pakistan, in 2012, and the M.S. and Ph.D. degrees in electrical engineering from Kunsan National University, South Korea, in 2018. From December 2018 to August 2022, he was an Assistant Professor with the Institute of Southern Punjab, Multan, Pakistan. He is currently a Postdoctoral Researcher with Chungnam National University, South Korea. His research interests include the design of electrical machines and power electronics.

TANVEER YAZDAN was born in Jampur, Punjab, Pakistan. He received the bachelor's degree in electrical engineering from the University of Engineering and Technology, Taxila, Pakistan, in 2010, and the M.S. and Ph.D. degrees in electrical engineering from Hanyang University, South Korea, in 2018. From 2010 to 2013, he was an Assistant Manager with Karachi-Electric Company, Pakistan. He is currently an Assistant Professor with The University of Lahore, Pakistan. His research interest includes the design and control of electrical machines.

MUDASSIR RAZA SIDDIQI was born in 1991. He received the bachelor's degree in electrical engineering from the University of Engineering and Technology, Taxila, Pakistan, in 2012, the M.S. degree in electrical engineering from the Energy Conversion System Laboratory, Hanyang University, South Korea, in 2017, and the Ph.D. degree from the Department of Electrical Engineering, Incheon National University, South Korea, in 2022.

From 2017 to 2018, he was a Researcher with Nex-M Protohouse, Ansan, South Korea. Since March 2022, he has been a Research Professor in electrical engineering with Incheon National University. His research interest includes the design and control of electric machines.

HAN-WOOK CHO (Member, IEEE) received the B.S., M.S., and Ph.D. degrees from Chungnam National University, Daejeon, South Korea, in 2002, 2004, and 2007, respectively. From September 2007 to August 2010, he was a Senior Researcher with the Korea Institute of Machinery and Materials. From 2016 to 2017, he was a Visiting Scholar with the Department of Electrical and Computing Engineering, University of Illinois Urbana–Champaign, Urbana, IL, USA. He is currently a Professor with the Department of Electrical, Electronics, and Communication Engineering Education, Chungnam National University.